View metadata, citation and similar papers at core.ac.uk

brought to you by CORE

provided by Boise State University - ScholarWorks

Boise State University
ScholarWorks

Mathematics Faculty Publications and Presentations

Department of Mathematics

6-1-2009

Finite-Difference and Pseudo-Sprectral Methods for the Numerical Simulations of In Vitro Human Tumor Cell Population Kinetics

Z. Jackiewicz
Arizona State University

Barbara Zubik-Kowal
Boise State University

B. Basse
University of Canterbury

This is an author-produced, peer-reviewed version of this article. The final, definitive version of this document can be found online at *Mathematical Biosciences and Engineering*, published by American Institute of Mathematical Sciences. Copyright restrictions may apply. DOI: 10.3934/mbe.2009.6.561

MATHEMATICAL BIOSCIENCES
AND ENGINEERING
Volume **X**, Number **0X**, XX **200X**

http://www.mbejournal.org/

pp. **X–XX**

FINITE-DIFFERENCE AND PSEUDO-SPECTRAL METHODS FOR THE NUMERICAL SIMULATIONS OF IN VITRO HUMAN TUMOR CELL POPULATION KINETICS

Z. Jackiewicz
Department of Mathematics and Statistics, Arizona State University
Tempe, Arizona 85287, USA

B. Zubik-Kowal
Department of Mathematics, Boise State University
1910 University Drive, Boise, Idaho 83725, USA

B. Basse
Department of Mathematics and Statistics, University of Canterbury
Private Bag 4800, New Zealand

Abstract. Pseudo-spectral approximations are constructed for the model equations which describe the population kinetics of human tumor cells in vitro and their responses to radiotherapy or chemotherapy. These approximations are more efficient than finite-difference approximations. The spectral accuracy of the pseudo-spectral method allows us to resolve the model with a much smaller number of spatial grid-points than required for the finite-difference method to achieve comparable accuracy. This is demonstrated by numerical experiments which show a good agreement between predicted and experimental data.

1. **Introduction.** Patient responses, and in some cases non-responses, to cancer therapies such as radiation, chemotherapy and combination treatments are not completely understood. In vitro studies have shown that therapies may target the cellular mechanisms of growth, division and death in all or some stages of the cell cycle [1]. Even in the simplified environment of the laboratory with modern techniques it is not always possible to isolate the effects of cancer treatment on the cell cycle of human cancer cell lines yet this is crucial if we are to understand drug mechanisms and patient responses to therapy.

With this in mind a mathematical model for the kinetics of a population of cells differentiated by phases of the cell division cycle and length of time within each phase has been developed and used to describe the effects of a number of cancer therapies in vitro ([2, 3, 4, 5, 6, 11, 7]). Validation of the model is achieved by comparing model and data flow cytometric profiles of human melanoma cell lines. Model parameters that cannot be determined experimentally are chosen to optimally fit model and data.

2000 *Mathematics Subject Classification.* Primary: 45K05, 34K28; Secondary: 62P10.

Key words and phrases. Population kinetics of human cancer cells in vitro, human tumor cells, cell cycle dynamics, mathematical model, pseudo-spectral methods, finite-difference methods.

Corresponding author: B. Zubik-Kowal. The work of Z. Jackiewicz was partially supported by NSF grants DMS-0509597 and DMS-0510813.

Flow cytometry is a technique where the DNA content of individual cells is measured and binned accordingly. The resulting histogram is termed a 'flow cytometric profile' and for cells unperturbed by therapy consists of two distinct peaks (Fig. 1) one with double the DNA content of the other. The tallest peak is the cluster of cells in the first phase of the cell cycle. The second peak, at double the DNA content of the first consists of cells that are nearing the end of the cell cycle and are about to divide. Perturbation by cancer therapy causes these peaks to change in relation to one another (Fig. 2). A mathematical model is the ideal tool for analysing flow cytometric profiles and isolating the underlying drug mechanisms.

Because optimisation routines require numerous model iterations, further applications of the model would be enhanced by finding an efficient numerical algorithm to solve the model. In this paper we summarize the model, then we apply both finite difference and pseudo-spectral methods for the numerical solution of the model. We conclude that, for the equations describing the population kinetics of human cancer cells in vitro, the pseudo-spectral method is more efficient than the finite difference method. Moreover, the difference in efficiency of both methods increases with increasing length of the time interval (domain of the time variable used in the model). This conclusion suggests the choice of the pseudo-spectral method for the estimation of the optimal parameter values which have to be found for the mathematical model.

The organization of this paper is as follows. In Section 2, we provide a mathematical description of the model equations. The processes of the spatial discretization of the model by the finite-difference and pseudo-spectral methods are then described in Sections 3 and 4, respectively. The numerical experiments with the model are presented in Section 5. Finally, in Section 6 some concluding remarks are given.

2. **Mathematical model.**

The cancer cell division cycle can be divided into four distinct phases, namely the G_1-phase, DNA synthesis or S-phase, G_2-phase, and mitosis or M-phase; see Fig. 1 of [2], which expresses the accumulation of cells in each of the phases and the movement of cells between them. The transitions between the G_1, S, G_2, M-phases are controlled by stochastic processes. The mathematical model, which was developed in [2], describes these phases and the transition rates between them, and is based on the system of partial differential equations of the form

$$\begin{cases} \dfrac{\partial G_1(x,t)}{\partial t} &= 4b\,M(2x,t) \;-\; (k_1+\mu_{G_1})\,G_1(x,t), \\ \dfrac{\partial S(x,t)}{\partial t} &= \varepsilon\,\dfrac{\partial^2 S(x,t)}{\partial x^2} \;-\; \mu_S\,S(x,t) \;-\; g\dfrac{\partial S(x,t)}{\partial x}, \\ &+\; k_1\,G_1(x,t) \;-\; I(x,t;T_S), \\ \dfrac{\partial G_2(x,t)}{\partial t} &= I(x,t;T_S) \;-\; (k_2+\mu_{G_2})\,G_2(x,t), \\ \dfrac{\partial M(x,t)}{\partial t} &= k_2\,G_2(x,t) \;-\; b\,M(x,t) \;-\; \mu_M\,M(x,t). \end{cases} \tag{2.1}$$

Here, $t \geq 0$ is time (measured in hours) and x is the dimensionless relative DNA content. The dependent variables, $G_1(x,t)$, $S(x,t)$, $G_2(x,t)$ and $M(x,t)$ represent the density of cells in the corresponding phases. The delay term $I(x,t;T_S)$ represents cells that have been in S-phase for T_S hours and are ready to be transferred to G_2-phase. The derivation of this term is explained in detail in [2]. In short

$I(x,t;T_S)$ is the solution of the diffusion equation

$$\frac{\partial I(x,t;\tau_S)}{\partial \tau_S} + g\frac{\partial I(x,t;\tau_S)}{\partial x} - \varepsilon\frac{\partial^2 I(x,t;\tau_S)}{\partial x^2} + \mu_S\, I(x,t;\tau_S) = 0, \quad 0 < x < \infty, \quad t > \tau_S > 0,$$

at time $\tau_S = T_S$ where τ_S is the time since arrival in S-phase. The analytical solution (with appropriate initial conditions and a zero flux boundary condition) is obtained using Laplace transform techniques and Green's functions. Thus $I(x,t;T_S)$ is given by

$$\begin{cases} I(x,t;T_S) = \displaystyle\int_0^\infty k_1\, G_1(y, t-T_S)\, \gamma(T_S,x,y)dy, & t \geq T_S, \\ I(x,t;T_S) = 0, & t < T_S, \end{cases} \tag{2.2}$$

where $\gamma(\tau,x,y)$ is a weight function given by

$$\begin{aligned} \gamma(\tau,x,y) &= \frac{\exp(-\mu_S\tau)}{2\sqrt{\pi\varepsilon\tau}}\left(\exp\left(-\frac{\big((x-g\tau)-y\big)^2}{4\varepsilon\tau}\right)\right. \\ &- \left.\big(1+\nu(\tau,x,y)\big)\exp\left(-\frac{\big(x+g\tau)+y\big)^2}{4\varepsilon\tau}\right)\right) \end{aligned} \tag{2.3}$$

with

$$\nu(\tau,x,y) = \frac{x+y}{g\tau}\Big(1+O(\tau^{-1}\Big).$$

Here γ is a Greens function and the ν term arises due to the zero flux boundary condition.

The parameters μ_{G_1}, μ_S, μ_{G_2}, and μ_M are the death rates in G_1, S, G_2, and M-phases, respectively. The parameters k_1 and k_2 are the transition probabilities of cells from G_1 to S-phase and from G_2 to M-phase, respectively; b is the division rate; ε is the dispersion coefficient; and g is the average growth rate of DNA in the S-phase. The $4b\,M(2x,t)$ term on the right hand side of the first equation in (2.1) arises due to a change of variable in the derivation as cells in an interval $[2x, 2x+2\Delta x]$ are doubled in number and transferred to the interval $[x, x+\Delta x]$ with half the DNA content.

In this paper, we consider constant parameters, like in [2], but in general, they all may be functions of either x or t, or both of these variables.

The system (2.1) is incomplete and should be supplemented with initial and boundary conditions. These side conditions, which are chosen according to experimental evidence, take the form

$$\begin{cases} G_1(x,0) = \dfrac{a_0}{\sqrt{2\pi\theta_0^2}}\exp\left(-\dfrac{(x-1)^2}{2\theta_0^2}\right), & 0 < x < \infty, \\ S(x,0) = 0, \quad G_2(x,0) = 0, \quad M(x,0) = 0, & 0 < x < \infty, \end{cases} \tag{2.4}$$

and

$$\varepsilon\,\frac{\partial S(0,t)}{\partial x} - g\,S(0,t) = 0, \quad t > 0. \tag{2.5}$$

Here, the initial DNA content of cells in the G_1-phase is chosen as a Gaussian distribution with relative mean DNA content at $x = 1$ equal to a_0, and variance θ_0^2. This variance is chosen sufficiently small so that the extension of $G_1(x,0)$ into the infeasible region $x < 0$ is of no significance.

In Sections 3 and 4 we construct numerical solutions to (2.1) supplemented by the initial condition (2.4) and the general boundary conditions of the form

$$\begin{cases} \varepsilon \dfrac{\partial S(0,t)}{\partial x} - g\, S(0,t) = \alpha, & t > 0, \\ S(L,t) = \beta, & t > 0, \end{cases} \tag{2.6}$$

with any real values α and β. The case $\alpha = 0$ corresponds to the zero flux condition (2.5). The parameter β can be chosen according to the experimental data provided in [2]. In Section 3 we investigate the finite-difference method while in Section 4 we investigate the pseudo-spectral method for the model equations (2.1). The pseudo-spectral method demonstrates better efficiency for the model (2.1) than the finite-difference method. This is illustrated by the results of numerical experiments presented in Section 5. Finally, in Section 6, some concluding remarks are given and plans for future research are briefly outlined.

3. **Finite difference spatial discretization of the model.** In this section we discretize the equation for S in (2.1) in space by the finite-difference method. For a given positive integer N let $\Delta x = L/N$ and define the uniform grid

$$x_i = (i-1)\Delta x, \quad i = 1, 2, \ldots, N+1.$$

Our choice of the finite-difference operator for the first order derivative $\partial S/\partial x$ in the advection-diffusion equation for the S-phase in (2.1) is dictated by the parameter values ε and g. Since the practical values of the parameter ε are arbitrarily close to zero and the practical values of the parameter g are isolated from zero, the so-called *cell Peclet number* $g\Delta x/\varepsilon$ is arbitrarily large. In this case the equation for S in (2.1) is *advection-dominated* and use of the second order central finite-difference operator for the first order derivative $\partial S/\partial x$ may lead to numerical oscillations if Δx is not depressed to very small values which lead to very expensive numerical solutions, see [9]. Therefore, for the first order spatial derivative in (2.1) we apply the approximations

$$\frac{\partial S(x_i,t)}{\partial x} \approx \frac{S(x_i,t) - S(x_{i-1},t)}{\Delta x}, \tag{3.1}$$

for $i = 2, 3, \ldots, N$. For $i = 1$ we apply the Neumann boundary condition in (2.6), which gives the exact value for the derivative at $x_1 = 0$

$$\frac{\partial S(x_1,t)}{\partial x} = \frac{g\, S(x_1,t) + \alpha}{\varepsilon}. \tag{3.2}$$

For the second order spatial derivative we apply the approximations

$$\frac{\partial^2 S(x_i,t)}{\partial x^2} \approx \frac{S(x_{i-1},t) - 2S(x_i,t) + S(x_{i+1},t)}{\Delta x^2}, \tag{3.3}$$

$i = 2, 3, \ldots, N$. For $i = 1$ we apply again the Neumann boundary condition in (2.6), which results in

$$\frac{\partial^2 S(x_1,t)}{\partial x^2} \approx \frac{1}{\Delta x}\left(\frac{S(x_2,t) - S(x_1,t)}{\Delta x} - \frac{g\, S(x_1,t) + \alpha}{\varepsilon} \right). \tag{3.4}$$

The Dirichlet condition in (2.6) gives

$$S(x_{N+1},t) = \beta. \tag{3.5}$$

Put

$$S(t) = \begin{bmatrix} S(x_1,t) \\ S(x_2,t) \\ \vdots \\ S(x_N,t) \end{bmatrix}, \quad \frac{dS(t)}{dt} = \begin{bmatrix} \frac{\partial S}{\partial t}(x_1,t) \\ \frac{\partial S}{\partial t}(x_2,t) \\ \vdots \\ \frac{\partial S}{\partial t}(x_N,t) \end{bmatrix},$$

$$r(t;T_S) = \begin{bmatrix} k_1 G_1(x_1,t) - I(x_1,t;T_S) \\ k_1 G_1(x_2,t) - I(x_2,t;T_S) \\ \vdots \\ k_1 G_1(x_N,t) - I(x_N,t;T_S) \end{bmatrix}, \quad v = \begin{bmatrix} \alpha\left(\frac{2}{\Delta x} + \frac{g}{\varepsilon}\right) \\ 0 \\ \vdots \\ 0 \end{bmatrix},$$

and

$$A = \begin{bmatrix} \hat{a} & 2c & 0 & \dots & \dots & 0 \\ \hat{b} & a & c & \ddots & & \vdots \\ 0 & \hat{b} & a & c & \ddots & \vdots \\ \vdots & \ddots & \ddots & \ddots & \ddots & 0 \\ \vdots & & \ddots & \hat{b} & a & c \\ 0 & \dots & \dots & 0 & \hat{b} & a \end{bmatrix},$$

with

$$a = -\frac{2\varepsilon}{\Delta x^2} - \frac{g}{\Delta x}, \quad \hat{a} = -\frac{2\varepsilon}{\Delta x^2} - \frac{2g}{\Delta x} - \frac{g^2}{\varepsilon}, \quad \hat{b} = \frac{\varepsilon}{\Delta x^2} + \frac{g}{\Delta x}, \quad c = \frac{\varepsilon}{\Delta x^2}.$$

Applying the approximations (3.1)-(3.4) to the equation for S in (2.1) results in the system of ordinary delay differential equations

$$\frac{dS(t)}{dt} = AS(t) - \mu_S S(t) + r(t;T_S) - v, \tag{3.6}$$

with the length T_S of the delay.

Since the right-hand sides of the equations for G_1, G_2 and M in (2.1) do not include partial derivatives in x, the semi-discrete equations for these variables take the following form

$$\begin{cases} \frac{dG_1(t)}{dt} &= 4b\, M^{(2)}(t) \;-\; (k_1 + \mu_{G_1})\, G_1(t), \\ \frac{dG_2(t)}{dt} &= I(t;T_S) \;-\; (k_2 + \mu_{G_2})\, G_2(t), \\ \frac{dM(t)}{dt} &= k_2\, G_2(t) \;-\; b\, M(t) \;-\; \mu_M\, M(t). \end{cases} \tag{3.7}$$

Here,

$$G_j(t) = \begin{bmatrix} G_j(x_1,t) \\ G_j(x_2,t) \\ \vdots \\ G_j(x_{N+1},t) \end{bmatrix},\ j = 1,2, \quad I(t;T_S) = \begin{bmatrix} I(x_1,t;T_S) \\ I(x_2,t;T_S) \\ \vdots \\ I(x_{N+1},t;T_S) \end{bmatrix},$$

$$M(t) = \begin{bmatrix} M(x_1,t) \\ M(x_2,t) \\ \vdots \\ M(x_{N+1},t) \end{bmatrix}, \quad M^{(2)}(t) = \begin{bmatrix} M_1^{(2)}(t) \\ M_2^{(2)}(t) \\ \vdots \\ M_{N+1}^{(2)}(t) \end{bmatrix},$$

where the values $M_i^{(2)}(t)$ are defined by

$$M_i^{(2)}(t) = \begin{cases} M(2x_i,t) & \text{if} \quad 2x_i \le L, \\ 0 & \text{if} \quad 2x_i > L, \end{cases}$$

according to the experimental data provided in [2].

The system of equations (3.6)-(3.7) create a finite-difference semi-discrete approximation for the whole model (2.1). The results of numerical experiments with (3.6)-(3.7) are presented in Section 5.

4. **Pseudo-spectral spatial discretization of the model.** In this section, to compute numerical approximations to the S-phase, we discretize the corresponding parabolic equation in (2.1) with respect to x by pseudo-spectral method based on the Chebyshev-Gauss-Lobatto points

$$x_i = \frac{L}{2}\left(1 - \cos\frac{(i-1)\pi}{N}\right),$$

for $i = 1, 2, \ldots, N+1$, on the interval $[0, L]$.

The first order spatial derivative which appears in the equation for S in (2.1) can be replaced by the spectrally accurate approximations at the spatial grid-points x_i

$$\frac{\partial S(x_i,t)}{\partial x} \approx \sum_{j=1}^{N} d_{ij} S(x_j,t) + \beta d_{i,N+1}, \tag{4.1}$$

for $i = 2, 3, \ldots, N+1$, where we incorporated the Dirichlet boundary condition (3.5). Here,

$$D^{(1)} = \Big[d_{ij}\Big]_{i,j=1}^{N+1}$$

is the differentiation matrix of the first order (see [8] and [12]). For $i = 1$ the first condition in (2.6) leads to

$$\frac{\partial S(x_1,t)}{\partial x} = \frac{g\, S(x_1,t) + \alpha}{\varepsilon} \tag{4.2}$$

as in the case of finite-difference approximation. The relations (4.1)-(4.2) result in the approximation

$$S_x(t) \approx D_0 S(t) + \beta d_{N+1}^{(0)} + b_1 e_1 \tag{4.3}$$

with the following notations

$$D_0 = \begin{bmatrix} 0 & 0 & \ldots & 0 \\ d_{21} & d_{22} & \ldots & d_{2,N} \\ \vdots & \vdots & \ddots & \vdots \\ d_{N,1} & d_{N,2} & \ldots & d_{N,N} \end{bmatrix}, \quad e_1 = \begin{bmatrix} 1 \\ 0 \\ \vdots \\ 0 \end{bmatrix},$$

$$S_x(t) = \begin{bmatrix} \dfrac{\partial S(x_1,t)}{\partial x} \\ \dfrac{\partial S(x_2,t)}{\partial x} \\ \vdots \\ \dfrac{\partial S(x_N,t)}{\partial x} \end{bmatrix}, \quad d_{N+1}^{(0)} = \begin{bmatrix} 0 \\ d_{2,N+1} \\ \vdots \\ d_{N,N+1} \end{bmatrix},$$

and

$$b_1 = \frac{g\, S(x_1,t) + \alpha}{\varepsilon}.$$

The second order spatial derivative which appears in the equation for S in (2.1) can also be replaced by spectrally accurate approximations at the spatial grid-points x_i. These approximations are written in the form

$$\frac{\partial^2 S(x_i,t)}{\partial x^2} \approx b_1 d_{i1} + \sum_{j=2}^{N+1} d_{ij} \frac{\partial S(x_j,t)}{\partial x}, \tag{4.4}$$

for $i = 1, 2, \ldots, N$. The relations (4.4), (4.3) and (4.1) result in the approximation

$$\begin{aligned} S_{xx}(t) &\approx DS_x(t) + \left(\sum_{j=1}^{N} d_{N+1,j} S(x_j,t) + d_{N+1,N+1}\beta \right) d_{N+1} \\ &\approx D\Big(D_0 S(t) + \beta d_{N+1}^{(0)} + b_1 e_1 \Big) \\ &+ \left(\sum_{j=1}^{N} d_{N+1,j} S(x_j,t) + d_{N+1,N+1}\beta \right) d_{N+1}, \end{aligned} \tag{4.5}$$

with the notations

$$S_{xx}(t) = \begin{bmatrix} \dfrac{\partial^2 S(x_1,t)}{\partial x^2} \\ \dfrac{\partial^2 S(x_2,t)}{\partial x^2} \\ \vdots \\ \dfrac{\partial^2 S(x_N,t)}{\partial x^2} \end{bmatrix}, \quad d_{N+1} = \begin{bmatrix} d_{1,N+1} \\ d_{2,N+1} \\ \vdots \\ d_{N,N+1} \end{bmatrix},$$

and

$$D = D^{(1)}(1:N, 1:N) = \begin{bmatrix} d_{11} & d_{12} & \ldots & d_{1,N} \\ d_{21} & d_{22} & \ldots & d_{2,N} \\ \vdots & \vdots & \ddots & \vdots \\ d_{N,1} & d_{N,2} & \ldots & d_{N,N} \end{bmatrix}.$$

The approximations (4.3) and (4.5) applied to the partial differential equation for S in (2.1) result in the following system of ordinary delay differential equations

$$\begin{aligned}\frac{dS(t)}{dt} &= \varepsilon\left(D\Big(D_0S(t)+\beta d^{(0)}_{N+1}+b_1e_1\Big)\right.\\ &+ \left.\Big(\sum_{j=1}^{N} d_{N+1,j}S(x_j,t)+d_{N+1,N+1}\beta\Big)d_{N+1}\right)-\mu_S\,S(t)\\ &- g\left(D_0S(t)+\beta d^{(0)}_{N+1}+b_1e_1\right)+r(t;T_S).\end{aligned} \tag{4.6}$$

with the length T_S of the delay.

As in Section 3 the system of equations (4.6) is supplemented with the system (3.7) which corresponds now to the Chebyshev-Gauss-Lobatto points x_i defined at the beginning of this section. This leads to the overall pseudo-spectral semi-discrete approximation for the whole model (2.1). The results of numerical experiments with this approximation (4.6), (3.7) are then presented in Section 5 and compared with experimental data.

5. **Numerical experiments.** In the previous two sections we described the algorithms for the discretization in space of the model equations (2.1)-(2.2). In Section 3 the equation for the variable $S(x,t)$ was discretized by finite-difference approximations (3.1)-(3.4) and in Section 4 by pseudo-spectral approximations (4.3) and (4.5). This leads to the overall systems of delay-differential equations (DDEs) (3.6)-(3.7) or (4.6)-(3.7), respectively. Here, the delay T_S enters the equations for $S(x,t)$ and $G_2(x,t)$ through the terms $r(t;T_S)$ with $I(x,t;T_S)$ defined by (2.2). The numerical solution of models similar to (2.1)-(2.2) by finite-difference methods is also briefly discussed in [6].

To solve the resulting systems of DDEs we first describe the algorithm for (3.7). This algorithm is based on backward differentiation method of the first order (BDF1) to compute the necessary starting values, followed by the backward differentiation method of order $p=3$ on the remainder of the interval of integration, applied to the system (3.7) reordered as follows

$$\begin{cases}\dfrac{dG_2(t)}{dt} &= I(t;T_S)\;-\;(k_2+\mu_{G_2})\,G_2(t),\\ \dfrac{dM(t)}{dt} &= k_2\,G_2(t)\;-\;b\,M(t)\;-\;\mu_M\,M(t),\\ \dfrac{dG_1(t)}{dt} &= 4b\,M^{(2)}(t)\;-\;(k_1+\mu_{G_1})\,G_1(t).\end{cases} \tag{5.1}$$

Then the algorithm based on BDF1 formula takes the form

$$\begin{cases}G_{2,n+1} &= \Big(1+\Delta t\Big(k_2+\mu_{G_2}\Big)\Big)^{-1}\Big(G_{2,n}+\Delta t I_{n+1-j}\Big),\\ M_{n+1} &= \Big(1+\Delta t\Big(b+\mu_M\Big)\Big)^{-1}\Big(M_n+k_2\Delta t G_{2,n+1}\Big),\\ G_{1,n+1} &= \Big(1+\Delta t\Big(k_1+\mu_{G_1}\Big)\Big)^{-1}\Big(G_{1,n}+4b\Delta t M^{(2)}_{n+1}\Big),\end{cases} \tag{5.2}$$

for $n = 0, 1, \ldots, n_{end}$. The algorithm based on BDF3 is the following

$$\left\{\begin{array}{rcl} G_{2,n+1} & = & \Big(11 + 6\Delta t\Big(k_2 + \mu_{G_2}\Big)\Big)^{-1}\Big(R_n(G_2) + 6\Delta t I_{n+1-j}\Big), \\ M_{n+1} & = & \Big(11 + 6\Delta t\Big(b + \mu_M\Big)\Big)^{-1}\Big(R_n(M) + 6k_2\Delta t G_{2,n+1}\Big), \\ G_{1,n+1} & = & \Big(11 + 6\Delta t\Big(k_1 + \mu_{G_1}\Big)\Big)^{-1}\Big(R_n(G_1) + 24b\Delta t M^{(2)}_{n+1}\Big), \end{array}\right. \tag{5.3}$$

with

$$R_n(f) = 18f_n - 9f_{n-1} + 2f_{n-2}, \quad n = 2, 3, \ldots, n_{end}.$$

Here, n_{end} is the integer such that $n_{end}\Delta t = t_{end}$, where t_{end} is the end of the time interval over which the system (3.7) has to be solved, and the vectors $G_{2,n}$, I_{n-j}, M_n, $M^{(2)}_n$, and $G_{1,n}$ are approximations to $G_2(n\Delta t)$, $I((n-j)\Delta t; T_S)$, $M_n(n\Delta t)$, $M^{(2)}_n(n\Delta t)$, and $G_1(n\Delta t)$, respectively. The approximations I_{n-j} to $I((n-j)\Delta t; T_S)$ are computed using the formula (2.2), where the approximations to $G_1(y, (n-j)\Delta t)$ are computed either from the initial condition (2.4) if $(n-j)\Delta t = 0$ or from the previous stages of computations if $(n-j)\Delta t > 0$. The positive integer j is chosen in such a way that

$$j\Delta t \le T_S < (j+1)\Delta t.$$

To approximate the integral in (2.2) which is defined over the infinite interval $(0, \infty)$ we use the property that the kernel function $\gamma(T_S, x, y)$ defined by (2.3) is negligible for all $x \in [0, L]$ and $y > L$. This leads to the approximation

$$\left\{\begin{array}{ll} I(x, t; T_S) \approx \displaystyle\int_0^L k_1\, G_1(y, t - T_S)\, \gamma(T_S, x, y) dy, & t \ge T_S, \\ I(x, t; T_S) = 0, & t < T_S. \end{array}\right. \tag{5.4}$$

The integral in (5.4) is then approximated by the composite trapezoidal rule defined on the uniform grid on the interval $[0, L]$.

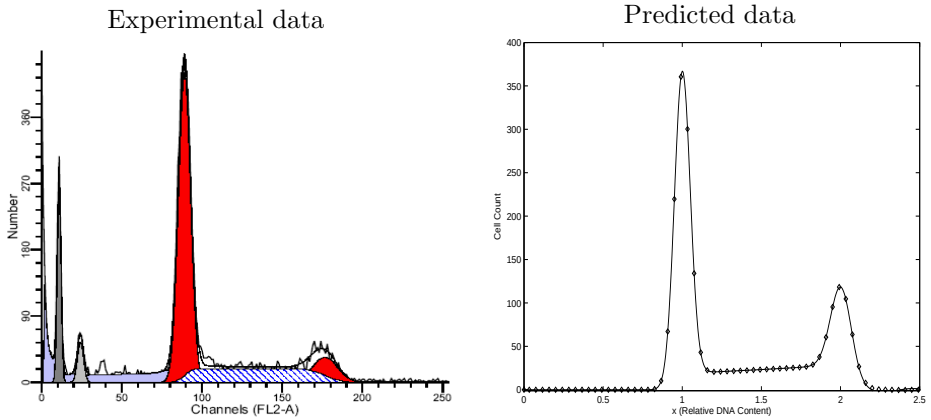

FIGURE 1. Cell count versus DNA content for an unperturbed cell line experimental (left) and predicted (right) data. The latter is $G_1(x, t) + S(x, t) + G_2(x, t) + M(x, t)$ at time $t = 12$.

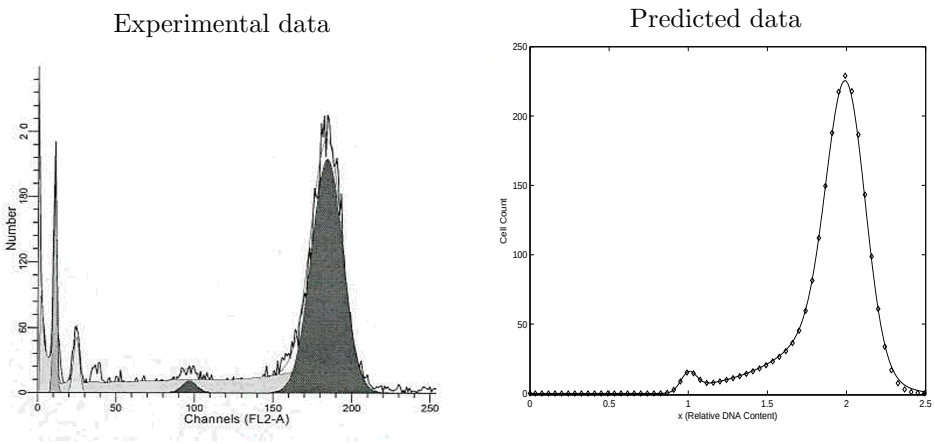

FIGURE 2. Cell count versus DNA content for a cell line perturbed by the anti-cancer drug Taxol which inhibits cell division. Experimental (left) versus predicted (right) data with the latter being $G_1(x,t) + S(x,t) + G_2(x,t) + M(x,t)$ at time $t = 72$.

Observe that the algorithm defined by (5.2) based on the BDF1 formula as well as the algorithm defined by (5.3) based on the BDF3 formula are explicit since all the values on the right hand sides of the corresponding equations are already known from previous stages of the computations. This means that although BDF1 and BDF3 are implicit methods, the algorithms (5.2) and (5.3) are explicit. Moreover, the stability advantages of BDF methods, which are expensive because of their impliciteness, are in this case for free if (5.2) and (5.3) are applied.

The remaining systems (3.6) or (4.6) resulting from semi-discretization in space of the variable $S(x,t)$ by finite-difference or pseudo-spectral methods, are then solved by the code `ode15s` from the *Matlab* ODE suite [10]. In this process the required terms $r(n\Delta t; T_S)$ are approximated using the values $G_{1,n}$ and I_{n-j}, $n = 0, 1, \ldots, n_{end}$, already computed by the algorithm described above for the numerical solution of (5.1).

The results of our numerical experiments are presented in Fig. 1 and Fig. 2 and compared with experimental data from [2]. In Fig. 1 we have the flow cytometric profile of a human cell line unperturbed by cancer therapy. In Fig. 1 the cell line has been perturbed by the anti-cancer trug Taxol which inhibits cell division and causes cells to build up in the G_2/M phase of the cell cycle.

The system (3.7) is solved by BDF3 with $\Delta t = 10^{-2}$ with starting values obtained using BDF1 formula. The system (3.6) was solved by the code `ode15s` with $N = 500$, $AbsTol = 10^{-5}$ and $RelTol = 10^{-1}$ for $t_{end} = 12$ and $t_{end} = 72$ and the numerical solutions are plotted by solid lines. For $t_{end} = 12$ there are 76 successful steps, 2 rejected steps, 599 function evaluations, 19 LU decompositions, and 97 solutions of linear systems. The time of integration is 12.24 *sec.* For $t_{end} = 72$ there are 92 successful steps, 0 rejected steps, 605 function evaluations, 11 LU decompositions, and 103 solutions of linear systems. The time of integration is 32.46 *sec.* The system (4.6) was solved by `ode15s` with $N = 80$, $AbsTol = 10^{-5}$ and $RelTol = 10^{-1}$ for the same values of $t_{end} = 12$ and $t_{end} = 72$ and the numerical solutions are displayed as the symbols '$\diamond$'. For $t_{end} = 12$ there are 129 successful

steps, 2 rejected steps, 381 function evaluations, 21 LU decompositions, and 155 solutions of linear systems. The time of integration is 3.48 *sec*, which is more than three times faster than the time of integration by the finite-difference method. For $t_{end} = 72$ there are 99 successful steps, 4 rejected steps, 400 function evaluations, 17 LU decompositions, and 155 solutions of linear systems. The time of integration is 7.52 *sec*, which is more than four times faster than the time of integration by the finite-difference method.

The pseudo-spectral method is more efficient than the method based on the finite-difference approach in spite of the fact that the pseudo-spectral method requires more steps and more function evaluations. This can be explained by the fact that the systems (4.6) have much smaller dimensions to achieve comparable accuracy and as the result these function evaluations are much less expensive for pseudo-spectral approach. Moreover, this difference in efficiency of pseudo-spectral methods as compared with finite-difference approximations increases as the length of the interval of integration increases.

6. **Discussion.** A new algorithm has been designed for a system of delay partial differential equations. The algorithm is based on pseudospectral approximations and has been investigated for the model equations (2.1)-(2.2) which describe the growth of human tumor cells and their responses to radiotherapy or chemotherapy. It has been demonstrated that the new algorithm for the numerical solution of (2.1)-(2.2) is more efficient than the standard algorithm based on the finite-difference approximations. The pseudo-spectral method requires much smaller number of grid-points than that needed for finite-difference method to reach comparable accuracy, and as a consequence the resulting pseudo-spectral semi-discrete systems are much smaller than the systems corresponding to finite-difference approximations. Discretization in time of the smaller pseudo-spectral systems is more robust and more efficient than discretization in time of the finite-difference systems. For the model equations integrated in time over the interval $[0, 12]$, the pseudo-spectral method is about three times more efficient than the finite-difference method and over the interval $[0, 72]$, the pseudo-spectral method is about four times more efficient than the finite-difference method. The difference in efficiency of these methods increases with increasing length of the time interval.

Our future work will address efficient numerical methods for estimating the parameter values of the model equations (2.1)-(2.2). These parameters have to be computed iteratively by minimizing the error between the numerical solution to (2.1)-(2.2) and the experimental data. Since this process usually has to be repeated several times the design of efficient numerical algorithms for (2.1)-(2.2) is very important. Therefore, we will adopt the pseudo-spectral algorithm to compare the numerical solutions with the experimental data. In order to obtain approximations to the model solutions as close as possible to the experimental data we will investigate the model equations for the parameters k_1, k_2, ε, g, b, μ_{G_1}, μ_S, μ_{G_2}, and μ_M belonging to different ranges. The numerical solutions computed for different sets of the parameters will be used to minimize the sum of squared errors on the appropriate grid. Since the pseudo-spectral algorithm is based on small numbers of grid-points, it will save the computational time for each solution computed for one set of the parameters.

Acknowledgements. With kind permission of Springer Science and Business Media, the two left-hand side pictures with experimental data in Fig. 1 and Fig. 2,

which were originally published in [2], are used here in this paper for comparison with our numerical data. We would like to thank Springer Science and Business Media for granting us their permission and making this comparison easier for the readers.

REFERENCES

[1] B. Alberts, A. Johnson, J. Lewis, M. Raff, K. Roberts and P. Walter, "Molecular Biology of the Cell", 4th ed., Garland, ISBN 0815332181, 2002.

[2] B. Basse, B.C. Baguley, E.S. Marshall, W.R. Joseph, B. van Brunt, G.C. Wake and D.J.N. Wall, *A mathematical model for analysis of the cell cycle in cell lines derived from human tumours*, J. Math. Biol. **47** (2003), 295–312.

[3] B. Basse, B.C. Baguley, E.S. Marshall, W.R. Joseph, B. van Brunt, G.C. Wake and D.J.N. Wall, *Modelling cell death in human tumour cell lines exposed to the anticancer drug paclitaxel*, J. Math. Biol., **49** (2004), 329–357.

[4] B. Basse, B.C. Baguley, E.S. Marshall, G.C. Wake and D.J.N. Wall, *Modelling cell population growth with applications to cancer therapy in human tumour cell lines*, Progress in Biophysics and Molecular Biology, **85** (2004), 353–368.

[5] B. Basse, G.C. Wake, D.J.N. Wall and B. van Brunt, *On a cell growth model for plankton, Mathematical Medicine and Biology*, A Journal of the IMA, **21** (2004), 49–61.

[6] B. Basse, B.C. Baguley, E.S. Marshall, G.C. Wake and D.J.N. Wall, *Modelling the flow cytometric data obtained from unperturbed human tumour cell lines: Parameter fitting and comparison*, Bulletin of Mathematical Biology, **67** (2005), 815–830.

[7] B. Basse and P. Ubezio, *A generalised age and phase structured model of human tumour cell populations both unperturbed and exposed to a range of cancer therapies*, Bulletin Mathematical Biology. Published Online First, (2007), DOI 10.1007/s11538-006-9185-6.

[8] C. Canuto, M.Y. Hussaini, A. Quarteroni and T.A. Zang, Spectral Methods in Fluid Mechanics, Springer Verlag, New York, 1988.

[9] W. Hundsdorfer, J. Verwer, Numerical Solution of Time-Dependent Advection-Diffusion-Reaction Equations, Springer-Verlag Berlin Heidelberg 2003.

[10] L.F. Shampine, M.W. Reichelt, The Matlab ODE suite, SIAM J. Sci. Comput. **18** (1997), 1-22.

[11] L. Spinelli, A. Torricelli, P. Ubezio and B. Basse, *Modelling the balance between quiescence and cell death in normal and tumour cell populations*, Mathematical BioSciences, **202** (2006), 349–370, doi:10.1016/j.mbs.2006.03.016

[12] Trefethen L.N., 2000, Spectral Methods in Matlab, SIAM, Philadelphia 2000.

E-mail address: zubik@math.boisestate.edu